Cellular/Molecular

# Role of Purinergic Receptor P2Y1 in Spatiotemporal $Ca^{2+}$ Dynamics in Astrocytes

Eiji Shigetomi,[1]* Yukiho J. Hirayama,[1]* Kazuhiro Ikenaka,[2] Kenji F. Tanaka,[3] and Schuichi Koizumi[1]

[1]Department of Neuropharmacology, University of Yamanashi, Yamanashi 409-3898, Japan, [2]Division of Neurobiology and Bioinformatics, National Institute for Physiological Sciences, Okazaki 444-8787, Japan, and [3]Department of Neuropsychiatry, School of Medicine, Keio University, Tokyo 160-8582, Japan

Fine processes of astrocytes enwrap synapses and are well positioned to sense neuronal information via synaptic transmission. In rodents, astrocyte processes sense synaptic transmission via Gq-protein coupled receptors (GqPCR), including the P2Y1 receptor (P2Y1R), to generate $Ca^{2+}$ signals. Astrocytes display numerous spontaneous microdomain $Ca^{2+}$ signals; however, it is not clear whether such signals are due to local synaptic transmission and/or in what timeframe astrocytes sense local synaptic transmission. To ask whether GqPCRs mediate microdomain $Ca^{2+}$ signals, we engineered mice (both sexes) to specifically overexpress P2Y1Rs in astrocytes, and we visualized $Ca^{2+}$ signals via a genetically encoded $Ca^{2+}$ indicator, GCaMP6f, in astrocytes from adult mice. Astrocytes overexpressing P2Y1Rs showed significantly larger $Ca^{2+}$ signals in response to exogenously applied ligand and to repetitive electrical stimulation of axons compared with controls. However, we found no evidence of increased microdomain $Ca^{2+}$ signals. Instead, $Ca^{2+}$ waves appeared and propagated to occupy areas that were up to 80-fold larger than microdomain $Ca^{2+}$ signals. These $Ca^{2+}$ waves accounted for only 2% of total $Ca^{2+}$ events, but they were 1.9-fold larger and 2.9-fold longer in duration than microdomain $Ca^{2+}$ signals at processes. $Ca^{2+}$ waves did not require action potentials for their generation and occurred in a probenecid-sensitive manner, indicating that the endogenous ligand for P2Y1R is elevated independently of synaptic transmission. Our data suggest that spontaneous microdomain $Ca^{2+}$ signals occur independently of P2Y1R activation and that astrocytes may not encode neuronal information in response to synaptic transmission at a point source of neurotransmitter release.

*Key words:* astrocyte; astrocyte process; ATP; calcium; GECI; P2Y1 receptor

**Significance Statement**

Astrocytes are thought to enwrap synapses with their processes to receive neuronal information via Gq-protein coupled receptors (GqPCRs). Astrocyte processes display numerous microdomain $Ca^{2+}$ signals that occur spontaneously. To determine whether GqPCRs play a role in microdomain $Ca^{2+}$ signals and the timeframe in which astrocytes sense neuronal information, we engineered mice whose astrocytes specifically overexpress the P2Y1 receptor, a major GqPCR in astrocytes. We found that overexpression of P2Y1 receptors in astrocytes did not increase microdomain $Ca^{2+}$ signals in astrocyte processes but caused $Ca^{2+}$ wavelike signals. Our data indicate that spontaneous microdomain $Ca^{2+}$ signals do not require activation of P2Y1 receptors.

## Introduction

Astrocytes are abundant cells in the brain and play many important roles in regulating neuronal functions, such as synapse formation, synaptic transmission, synaptic plasticity, and synapse remodeling (Sofroniew and Vinters, 2010; Araque et al., 2014; Volterra et al., 2014). Astrocytes express a plethora of Gq-protein coupled receptors (GqPCRs) for neurotransmitters, which are thought to be important for receiving information from neurons (Agulhon et al., 2008). Accumulating evidence indicates that increases in neuronal activities trigger $Ca^{2+}$ signals in astrocytes through GqPCRs, both *in vitro* and *in vivo* (Agulhon et al., 2008; Takata et al., 2011; Navarrete et al., 2012; Ding et al., 2013; Pauk-

Received Sept. 11, 2017; revised Dec. 6, 2017; accepted Dec. 18, 2017.

Author contributions: E.S. and S.K. designed research; E.S. and Y.J.H. performed research; K.I. and K.F.T. contributed unpublished reagents/analytic tools; E.S. and Y.J.H. analyzed data; E.S. and S.K. wrote the paper.

This work was supported by JSPS Grants-in-aid for Scientific Research (KAKENHI) on Innovative areas "Glial assembly" (JP25117003 to S.K.) and Grant-in-Aid for Young Scientists (A) (JP2571005 to E.S.) and Grant-in-Aid for Young Scientists (Start-up) (JP2480029 to E.S.), the Takeda Science Foundation (to E.S.), and the Uehara Memorial Foundation (to E.S.). We thank Yasuko Fukasawa, Makiko Tachibana, Akemi Kunugi, and Ryohei Komatsu for technical assistance; all members of the S.K. laboratory for stimulating discussions; and Dr. Jeremy Allen (Edanz Group; www.edanzediting.com/ac) for editing a draft of this manuscript.

The authors declare no competing financial interests.

*E.S. and Y.J.H. contributed equally to this study.

Correspondence should be addressed to Dr. Schuichi Koizumi, Department of Neuropharmacology, University of Yamanashi, Yamanashi, 1110 Shimokato, Chuo, Yamanashi 409-3898, Japan. E-mail: skoizumi@yamanashi.ac.jp.

DOI:10.1523/JNEUROSCI.2625-17.2017

 0270-6474/18/381383-13$15.00/0

ert et al., 2014; Srinivasan et al., 2015; Monai et al., 2016). It has been proposed that $Ca^{2+}$ elevation in astrocytes regulates synapses by regulating neurotransmitter uptake, ion uptake, and gliotransmitter release (Araque et al., 2014).

Astrocyte processes are proposed to be integral parts of neuronal circuits. Their processes enwrap synapses and are important for the regulation of synaptic transmission through transmitter uptake and gliotransmitter release (Araque et al., 2014). $Ca^{2+}$ imaging of astrocytes indicates that they produce microdomain $Ca^{2+}$ signals, which are elicited by activation of GqPCRs. Astrocyte processes are able to respond to synaptic information at the point source of neurotransmitter release via GqPCRs, which contributes to the regulation of basal synaptic transmission through $Ca^{2+}$-dependent gliotransmission (Di Castro et al., 2011; Panatier et al., 2011).

Recent $Ca^{2+}$ imaging in rodent astrocytes revealed numerous microdomain $Ca^{2+}$ signals that occur spontaneously both *in vitro* and *in vivo* (Di Castro et al., 2011; Gee et al., 2014; Haustein et al., 2014; Kanemaru et al., 2014; Rungta et al., 2016; Agarwal et al., 2017). However, these $Ca^{2+}$ microdomains are insensitive to GqPCR antagonists. They are also reduced but still observed in *Itpr2*$^{-/-}$ mice, in which astrocytes lack a major pathway for $Ca^{2+}$ signals via GqPCRs (Haustein et al., 2014; Kanemaru et al., 2014; Srinivasan et al., 2015; Rungta et al., 2016; Agarwal et al., 2017). It is, therefore, not clear whether, when, and how astrocytes encode neuronal information to cause $Ca^{2+}$ signals. To understand how synapses are regulated by astrocyte processes, it is important to determine how astrocytes encode local neuronal information, whether astrocytes regulate local synaptic transmission and whether astrocytes regulate synapses bidirectionally through local control (Araque et al., 2014).

To investigate whether microdomain $Ca^{2+}$ signals are mediated by GqPCRs in astrocyte processes, we focused on astrocytes in the molecular layer (ML) of the DG because structural evidence indicates that most synapses (~90%) are ensheathed by astrocyte processes (Bosch et al., 2016) and activation of P2Y1 receptor (P2Y1R), a metabotropic receptor for extracellular ATP, leads to microdomain $Ca^{2+}$ signals at astrocyte processes in the ML of the DG (Santello et al., 2011). Expression of P2Y1R is not specific to astrocytes. Neurons also express P2Y1Rs in the hippocampus (Bowser and Khakh, 2004; Kawamura et al., 2004). To directly test whether P2Y1Rs contribute to microdomain $Ca^{2+}$ signals in astrocytes, we engineered mice whose astrocytes specifically overexpress P2Y1Rs. We then monitored microdomain $Ca^{2+}$ signals in astrocytes using GCaMP6f, a genetically encoded $Ca^{2+}$ indicator (GECI) (Chen et al., 2013; Haustein et al., 2014). We found that overexpression of P2Y1Rs enhanced responses to exogenous and endogenous ligands. However, we did not find evidence for microdomain $Ca^{2+}$ signals being increased or enhanced by overexpression of P2Y1Rs. Instead, the increased number of P2Y1Rs led to action potential-independent $Ca^{2+}$ wavelike signals, which encompassed significantly larger areas. These $Ca^{2+}$ waves were far fewer but larger and lasted longer than microdomain $Ca^{2+}$ signals. Our data indicate that spontaneous microdomain $Ca^{2+}$ signals occur independently of P2Y1R activation and that astrocytes may encode neuronal information when synapses are highly active but not in response to synaptic transmission at a point source of neurotransmitter release.

## Materials and Methods

*Animals.* All procedures were performed in accordance with the *Guiding principles for the care and use of animals in the field of physiologic sciences* published by the Physiologic Society of Japan and with the previous approval of the Animal Care Committee of Yamanashi University (Chuo, Yamanashi, Japan; Approval #A23-9). To express P2Y1R specifically in astrocytes, we took a transgenic approach using the Tet-OFF system (Tanaka et al., 2010; Shinozaki et al., 2017). Two lines of transgenic line were crossed: *Mlc1*-tTA and *P2ry1*$^{tetO}$. Double transgenic mice are referred to as P2Y1OE. *Mlc1* is specifically expressed in astrocytes. P2Y1R expression is induced under the control of the *Mlc1* promoter. Mice were housed on a 12 h light (6:00 A.M.)/dark (6:00 P.M.) cycle with *ad libitum* access to water and rodent chow. Both male and female mice were used. Genotyping PCR was performed using DNA purified from tail biopsies. The PCR primers used were as follows: *P2ry1*$^{tetO}$ forward, 5′-GTAGG CGTGTACGGTGGAG-3′; *P2ry1*$^{tetO}$ reverse, 5′-TGCAGTTGAGGCG ACAGTAC-3′; *Mlc1*-tTA forward, 5′-AAATTCAGGAAGCTGTGTGCC TGC-3′; and *Mlc1*-tTA reverse, 5′-CGGAGTTGATCACCTTGGAC TTGT-3′.

*ISH.* A 675 bp DNA fragment corresponding to the nucleotide positions 1100–1774 of mouse *P2ry1* (NM_008772.5) was subcloned into pGEMT-Easy vector (Promega) and was used for generation of sense or antisense RNA probes. RNA probes were synthesized using a DIG RNA labeling kit (Roche Diagnostics). Hybridization was performed using the ISH reagent kit (Genostaff; catalog #SRK-1) according to the manufacturer's instructions. The mouse brain tissues were fixed with Tissue Fixative (Genostaff; STF-01), embedded in paraffin using tissue processor CT-Pro20 (Genostaff), and sectioned at 6 $\mu$m. The sections were deparaffined with xylene and rehydrated through an ethanol series and PBS. The sections were fixed 10% neutral buffered formalin (10% formalin in PBS) for 15 min at room temperature (RT) and then washed with PBS. The sections were treated with 4 $\mu$g/ml ProteinaseK in PBS for 10 min at 37°C, washed with PBS, refixed with 10% neutral buffered formalin for 15 min at RT, again washed with PBS, and placed in 0.2 N HCl for 10 min at RT. After washing with PBS, the sections were placed in 1× G-WASH (Genostaff), equal to 1× SSC. Hybridization was performed with probes at concentrations of 300 ng/ml in G-Hybo (Genostaff) for 16 h at 60°C. After hybridization, the sections were washed in 1× G-WASH for 10 min at 60°C, 50% formamide in 1× G-WASH for 10 min at 60°C. Then the sections were washed twice with 1× G-WASH for 10 min at 60°C, twice 0.1× G-WASH for 10 min at 60°C, and twice with TBST (0.1% Tween 20 in TBS) at RT. After treatment with 1× G-Block (Genostaff) for 15 min at RT, the sections were incubated with anti-DIG AP conjugate (Roche Diagnostics) diluted 1:2000 with ×50G-Block (Genostaff) in TBST for 1 h at RT. The sections were washed twice with TBST and then incubated in 100 mM NaCl, 50 mM $MgCl_2$, 0.1% Tween 20, 100 mM Tris-HCl, pH 9.5. Coloring reactions were performed with NBT/BCIP solution (Sigma-Aldrich) overnight and then washed with PBS. The sections were counterstained with Kernechtrot stain solution (Muto Pure Chemicals) and mounted with G-Mount (Genostaff). For immunohistochemistry, tissue sections were deparaffined with xylene and rehydrated through an ethanol series and PBS. Antigen retrieval was performed by heat treatment by microwave for 20 min with citrate buffer, pH 6.0. Endogenous peroxidase was blocked with 0.3% $H_2O_2$ in methanol for 30 min, followed by incubation with Protein Block (Genostaff) and avidin/biotin blocking kit (Vector Laboratories). The sections were incubated with anti-GFAP rabbit polyclonal antibody (Dako; RRID:AB_10013382) at 4°C overnight. They were incubated with biotin-conjugated goat anti-rabbit IgG (Dako; RRID:AB_2313609) for 30 min at RT followed by the addition of peroxidase-conjugated streptavidin (Nichirei Biosciences) for 5 min. Peroxidase activity was visualized by diaminobenzidine. The sections were counterstained with Mayer's Hematoxylin (Muto Pure Chemicals), dehydrated, and then mounted with Malinol (Muto Pure Chemicals).

*Immunohistochemistry.* Brains were fixed with 4% PFA through cardiac perfusion. After postfixation in 4% PFA for 12–14 h, brains were subsequently submerged in 30% sucrose in PBS. Frozen 20 $\mu$m sections were cut with a cryostat (Leica Microsystems). Slices were washed with PBS three times and treated with 0.5% Triton X-100/10% normal growth serum for 1 h. After three washes with PBS, sections were incubated with chicken anti-GFP antibody (1:1000, Thermo Fisher Scientific; RRID: AB_2534023) and rat anti-GFAP antibody (1:2000, Thermo Fisher Scientific; RRID:AB_2532994) for 2 d. Sections were then washed three times with PBS and treated with fluorescent secondary antibodies (anti-

chicken IgY Alexa-488, 1:500, Thermo Fisher Scientific; RRID:AB_2534096; and anti-rat IgG Alexa-568, 1:500, Thermo Fisher Scientific; RRID: AB_2534125) for 2 h. After washing with PBS three times, sections were mounted on slides. Images were captured using a Fluoview 1200 (Olympus) equipped with a 40× silicon oil-immersion lens (N.A. 1.25).

*Microinjections of AAV 2/5.* Male and female transgenic mice were used in all experiments in accordance with the guidelines of the University of Yamanashi. Mice 6–9 weeks of age were anesthetized with isoflurane (induction at 5%, maintenance at 1.5%–3.0% v/v). All surgical procedures were conducted under general anesthesia using continuous isoflurane (1.5%–3.0%). Depth of anesthesia was monitored continuously and adjusted when necessary to ensure that animals were always anesthetized. Following induction of anesthesia, the mice were fitted into a stereotaxic frame with their heads secured by blunt ear bars and their noses placed into an anesthesia and ventilation system. The mice were administered 0.1 ml carprofen (Rimadyl, 5 mg/ml) subcutaneously before surgery for pain relief. The surgical incision site was cleaned three times with 10% povidone iodine and 70% ethanol. Skin was treated with 2% Xylocaine Jelly for pain relief. Skin incisions were made, followed by periosteum removal after applying 1% lidocaine (Xylocaine, 10 mg/ml). Craniotomies of ~2 mm in diameter were made above the left parietal cortex using a small (0.4 mm) steel burr (Minitor) powered by a high-speed drill (Minimo, Minitor). ACSF was composed of the following (in mM): 125 NaCl, 2.5 KCl, 1 $MgCl_2$, 2 $CaCl_2$, 10 HEPES, pH 7.2, ~310 mOsm, applied onto the skull to reduce heating caused by drilling. Unilateral viral injections were performed using beveled glass pipettes (1B100-4, WPI; 35°, outer diameter, ~28 μm) driven by a syringe pump (UMP-3+micro4, WPI). The 500–600 nl of AAV2/5 GfaABC1D cyto-GCaMP6f ($1.8 \times 10^{13}$ GC/ml, Penn Vector Core, Philadelphia) was injected unilaterally into the left hippocampus (2 mm posterior to bregma, 1 mm lateral to midline, 2 mm from the pial surface) at a speed of 0.2 μl/min. The glass pipettes were left in place for at least 10 min following each injection to minimize back flow of viral solution. Surgical wounds were closed with single external 5–0 nylon sutures (Akiyama Medical). Following surgery, animals were allowed to recover in cages placed partially on a low-voltage heating pad. Carprofen was administered once per day for up to 3 d after surgery. In addition, enrofloxacin (Baytril, 85 mg per 1l water) was dispensed in the drinking water to prevent infections until the mice were used. Hippocampal slices (300 μm) were cut and imaged 16–27 d after surgery.

*Preparation of brain slices and $Ca^{2+}$ imaging.* To minimize damage during the brain slicing procedure, we followed the protocol of Ting et al. (2014). Briefly, mice of either sex were anesthetized with pentobarbital (50 mg/kg, i.p.) or isoflurane (~2% v/v). Cold-cutting ACSF was composed of the following (in mM): 92 NaCl, 2.5 KCl, 1.2 $NaH_2PO_4$, 30 $NaHCO_3$, 20 HEPES, 25 D-glucose, 5 sodium ascorbate, 2 thiourea, 3 sodium pyruvate, 10 $MgCl_2$, and 0.5 $CaCl_2$, saturated with 95% $O_2$-5% $CO_2$, was perfused transcardially. Coronal slices of hippocampus (300 μm) were cut on a vibrating microtome (Pro7, Dosaka) in cutting ACSF. Slices were incubated at 34°C for 10 min in recovery ACSF composed of the following (in mM): 93 NMDG, 93 HCl, 2.5 KCl, 1.2 $NaH_2PO_4$, 30 $NaHCO_3$, 20 HEPES, 25 D-glucose, 5 sodium ascorbate, 2 thiourea, 3 sodium pyruvate, 10 $MgCl_2$, and 0.5 $CaCl_2$, saturated with 95% $O_2$-5% $CO_2$, and subsequently stored in ACSF comprised of the following (in mM): 124 NaCl, 2.5 KCl, 1.2 $NaH_2PO_4$, 24 $NaHCO_3$, 5 HEPES, 12.5 D-glucose, 5 sodium ascorbate, 2 thiourea, 3 sodium pyruvate, 2 $MgCl_2$, and 2 $CaCl_2$, saturated with 95% $O_2$ and 5% $CO_2$ at room temperature. After 1 h of recovery, slices and submerged in ACSF at ~32C°. Slices were imaged using a Fluoview FVMPE-RS two-photon laser scanning microscope (Olympus) equipped with Maitai HP DS-OL (Spectra-Physics). We used the laser at 920 nm (~8% power) and a 510 nm high pass emission filter. Astrocytes were selected from the ML of the dentate gyrus and were typically 50 μm from the slice surface. Images were gathered with a 25× water-immersion lens with a numerical aperture of 1.05 (Olympus). For electrical filed stimulation (EFS) experiments, a concentric bipolar stimulus electrode (IMB-160820, Intermedical, interpolar distance, 10 μm) was placed on the perforant path of the dentate gyrus. EFS (pulse duration, 100 μs) was delivered by a stimulus Isolator (Iso-Flex, A.M.P.I.,) and controlled by a stimulator (Master9, A.M.P.I.).

*Data analysis.* Slow drifts in astrocyte position (~2–5 μm) in the time lapse images were corrected with the TurboReg Plugin in NIH ImageJ (Thévenaz et al., 1998). We performed $Ca^{2+}$ imaging experiments in a single optical plane. $Ca^{2+}$ transients were measured by plotting the intensity of regions of interest (ROIs) over time, after the intensity of the background had been subtracted. ROIs were selected from somatic regions or process regions by visual examination of the time lapse image. Using these ROIs, raw fluorescence intensity values (F) were taken from the original videos and converted to Δ F/F (dF/F) in Originlab. A signal was declared a $Ca^{2+}$ transient if it exceeded the baseline by five times that of the baseline SD. Experiments for Figures 4 and 5 were performed with 3× zoom. The pixel unit was 0.3315 μm/pixel. For picking up areas displaying $Ca^{2+}$ signals, images were filtered using a median filter (radius, 2 pixels) to reduce noise. dF images were generated by subtraction of a median image from original F images. F exceeding >40 arbitrary units (a.u.), which corresponded to 0.1 dF/F, was defined as a $Ca^{2+}$ signal. Areas >1 μm were selected using the Fiji "Analyze particles" function. To define the initial sites of $Ca^{2+}$ waves, we analyzed the centroids of the events. When the centroid of $Ca^{2+}$ event was close enough (~2 μm) to either of readily distinguished structures, we defined them as events derived from such structures. We defined the rest of them as $Ca^{2+}$ events from fine processes. In some cases, the initial events were too large to define the initial sites reliably. When the area of the initial events exceeded 300 $\mu m^2$, we defined them as "unidentified" events; ~70% of initial events were <300 $\mu m^2$.

Data were analyzed using Originlab 8, 9, or 2016 (Origin Laboratory) and ImageJ (National Institutes of Health).

*Chemicals.* All reagents were from Thermo Fisher Scientific, Sigma-Aldrich, Tocris Bioscience, Abcam, Nacarai-Tesque, or Wako Chemicals.

*Experimental design and statistical analysis.* No statistical methods were used to predetermine sample size, but our sample sizes were consistent with those used in similar studies. FOVs that included morphologically unhealthy cells were excluded. Mice were randomly assigned to experiments. Data collection and analysis were not performed blind to experimental conditions. One mouse for each genotype was used for ISH in Figure 1*A*, *B*. Four mice were used for immunohistochemistry of GFAP and GFP in Figure 1*C*, *D*. Three mice were used for MRS 2365-evoked $Ca^{2+}$ signals in Figure 2*A*–*C*. Three mice were used for EFS-evoked $Ca^{2+}$ signals in Figure 2*F*. Two mice were used for EFS-evoked $Ca^{2+}$ signals in Figure 2*G*. Three control mice and six P2Y1OE mice were used for microdomain $Ca^{2+}$ signals in Figures 3 and 4. Two P2Y1OE mice were used for MRS 2179 treatment in Figure 5. Three (CPA) to four (TTX, carbenoxolone [CBX], probenecid [PB]) mice were used for pharmacological analysis of $Ca^{2+}$ waves in Figure 6. The number of acute slices used were described in Results. Statistical comparisons were made using the Mann–Whitney test, unpaired Student's *t* test, or paired Student's *t* test after analyzing the raw data to check whether they were normally distributed. The Kolmogorov–Smirnov test was used to compare the distributions of two groups. Data are shown as the mean ± SEM. Statistical tests were performed in InStat version 3.06 (GraphPad Software) or Origin 2016.

## Results

### Overexpression of P2Y1R specifically in astrocytes

We used the Tet-off system to overexpress *P2ry1* specifically into astrocytes. As such, we crossed the *Mlc1*-tTA-line, which is an astrocytic driver line (Tanaka et al., 2010) with the *P2ry1*$^{tetO}$ line. To confirm overexpression of *P2ry1*, we performed ISH and found strong signals in P2Y1R overexpression (P2Y1OE) mouse astrocytes (Fig. 1*A*). *P2ry1* mRNA signals were observed throughout the hippocampus. Strong signals were observed in the striatum radiatum in CA1 regions, and in the ML of the DG where many astrocytes are found. The strong ISH signals were colocalized with GFAP immunohistochemical signals (Fig. 1*B*), suggesting that astrocytes overexpressed *P2ry1*.

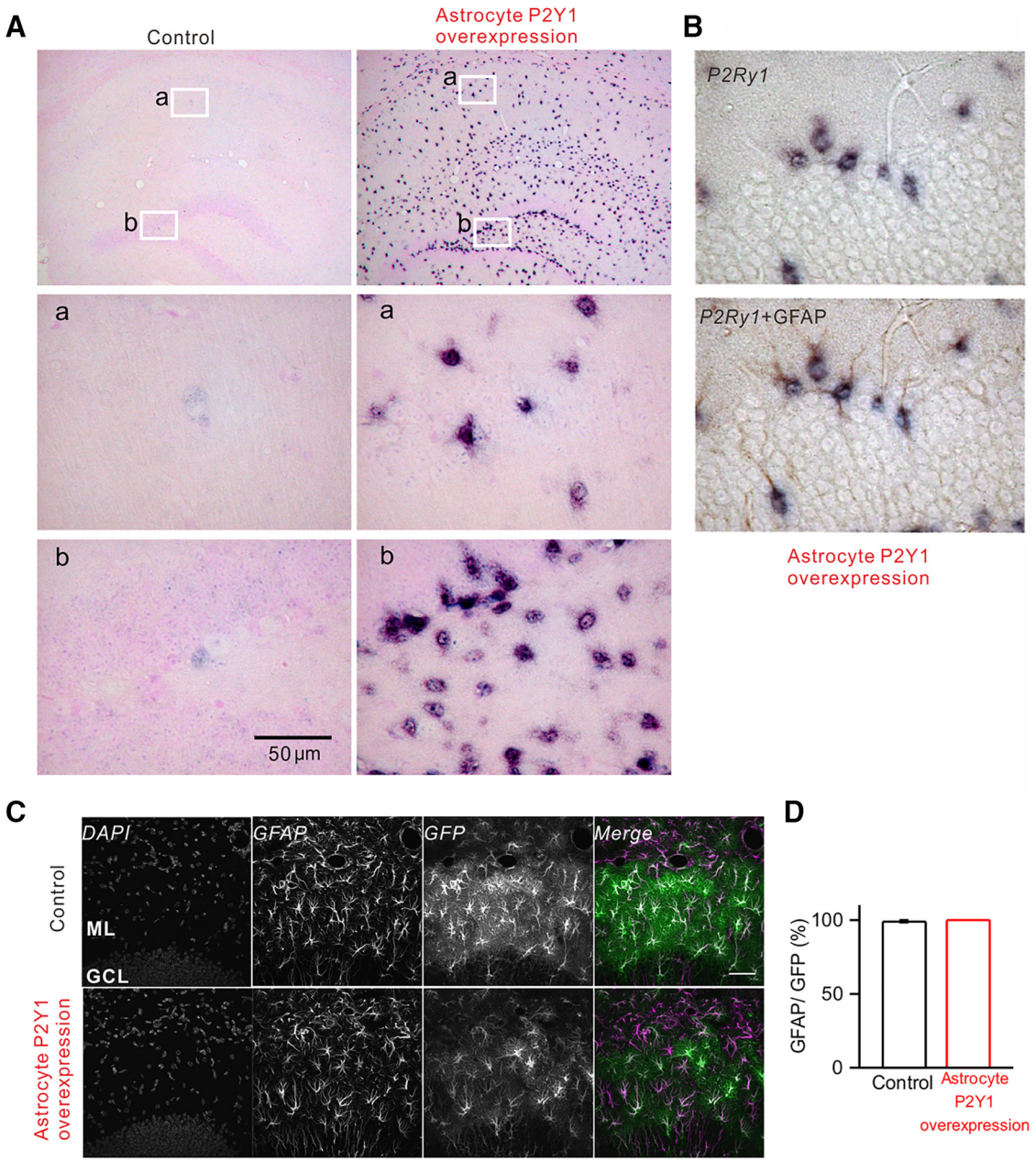


**Figure 1.** Astrocyte-specific overexpression of *P2ry1* and astrocyte-specific expression of GCaMP6f. ***A***, ISH of *P2ry1*. Bottom images, Dark signals represent *P2ry1* mRNA. These signals colocalize with GFAP immunostaining, suggesting astrocyte-specific overexpression of *P2ry1* (***B***). ***C***, Astrocyte-specific GCaMP6f expression. Immunohistochemistry for GFAP and GFP (for GCaMP6f). ***D***, Summary of immunohistochemistry. Almost all GFP-positive cells (i.e., GCaMP6f-expressing cells) were GFAP-positive astrocytes.

### Functional upregulation of P2Y1R-mediated $Ca^{2+}$ signals in astrocytes overexpressing P2Y1Rs

We asked whether *P2ry1* overexpression leads to expression of functional P2Y1R proteins. To confirm expression of functional P2Y1Rs, we performed $Ca^{2+}$ imaging to observe P2Y1R-mediated $Ca^{2+}$ signals in acute brain slices. We mainly focused on the ML of the DG because P2Y1R-mediated $Ca^{2+}$ signals are well characterized in this region (Jourdain et al., 2007; Di Castro et al., 2011; Santello et al., 2011), and astrocyte processes have been shown to closely ensheath synapses (Bosch et al., 2016). We injected AAV2/5 gfaABC1D cyto-GCaMP6f (Haustein et al., 2014) into the DG. GCaMP6f fluorescence was observed in the ML and hilus but not in the GCL. Immunohistochemical analysis showed that GCaMP6f expression was observed in the entire ML of the DG, and almost all GCaMP6f-expressing cells were GFAP-positive astrocytes (Fig. 1*C*,*D*; Control, 99 ± 1%; P2Y1OE, 100 ± 0%) which is consistent with previous studies (Haustein et al., 2014; Srinivasan et al., 2015). To see whether P2Y1R-mediated $Ca^{2+}$ signals were augmented, MRS 2365 (1 $\mu$M for 1 min), a P2Y1R selective agonist, was applied to the bathing medium. $Ca^{2+}$ elevation was observed in both control and P2Y1OE slices (Fig. 2*A*). More astrocytes responded to MRS 2365 in P2Y1OE compared with control slices (Fig. 2*B*; Control, 47 ± 7%, $n = 13$ slices; P2Y1OE, 94 ± 2%, $n = 13$ slices, $U = 0$, $p = 0.000013$, Mann–Whitney test). The dF/F of signals was also larger in P2Y1OE compared with control slices (Fig. 2*C*; Control, 3.0 ± 0.4, $n = 53$ from 13 slices; P2Y1OE, 6.6 ± 05, $n = 102$ from 13 slices, $U = 1325$, $p = 2 \times 10^{-6}$, Mann–Whitney test). These

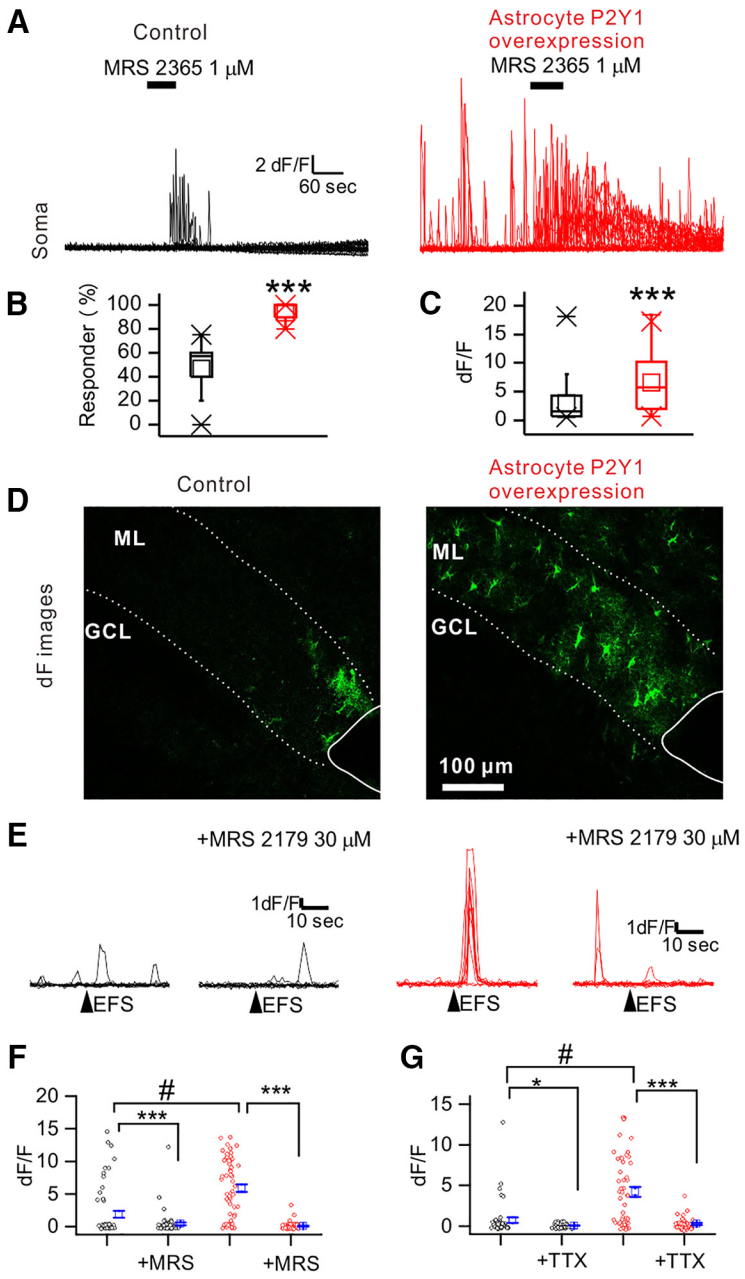


**Figure 2.** Functional assay for overexpression of P2Y1 receptor in astrocytes. ***A***, P2Y1 receptor agonist, MRS 2365 (1 $\mu$M), induced $Ca^{2+}$ signals in astrocytes. MRS 2365 was applied for 1 min as indicated by bars. P2Y1OE astrocytes showed larger signals. ***B***, Summary of response to MRS 2365. The ~94% of P2Y1OE astrocytes showed $Ca^{2+}$ responses to MRS 2365. ***C***, Summary of peak dF/F of MRS 2365-induced $Ca^{2+}$ signals. ***D***, EFS (40 Hz, 5 s, 0.1 mA)-evoked $Ca^{2+}$ signals. Images represent fluorescence just after stimulation. More astrocytes lit up in P2Y1OE slices. ***E***, Representative traces of intensity versus time profile of GCaM6f signals. EFS was applied at the points indicated by arrowheads. MRS 2179 (30 $\mu$M), a P2Y1 receptor antagonist, almost completely abolished the EFS-evoked $Ca^{2+}$ signals. ***F***, Summary of the effect of MRS 2179 on peak dF/F. ***G***, Summary of peak dF/F of EFS-evoked $Ca^{2+}$ signals. $Ca^{2+}$ signals in P2Y1OE astrocyte were significantly larger compared with control. TTX inhibited EFS-evoked $Ca^{2+}$ signals. $^{*}p < 0.05$, $^{***}p < 0.001$, $^{\#}p < 0.001$.

data suggest upregulation of functional P2Y1Rs in astrocytes of P2Y1OE mice. The overall time course of $Ca^{2+}$ elevation was similar between soma and processes, suggesting that P2Y1Rs are expressed in all astrocyte territories (data not shown).

In P30-P40 mice, astrocytes in the ML of the DG respond to synaptic transmission to elevate $Ca^{2+}$ in astrocyte processes (Di Castro et al., 2011). We asked whether overexpression of P2Y1Rs in astrocytes causes greater $Ca^{2+}$ signals in response to synaptic transmission. To elicit synaptic transmission, we performed EFS of the perforant path at 40 Hz (0.1 mA; Fig. 2*D*). Astrocytes showed larger EFS-evoked $Ca^{2+}$ signals in P2Y1OE compared with control slices (Fig. 2*E*,*F*; Control, 1.9 ± 0.4, $n$ = 58 astrocytes from 5 slices; P2Y1OE, 5.9 ± 0.6, $n$ = 56 astrocytes from 5 slices, $U$ = 690, $p = 1 \times 10^{-6}$, Mann–Whitney test). The distance over which astrocytes displayed evoked $Ca^{2+}$ signals was significantly greater in P2Y1OE compared with control slices (Fig. 2*D*; Control, 171 ± 26 $\mu$m, $n$ = 14 astrocytes; P2Y1OE, 274 ± 16 $\mu$m, $n$ = 42 astrocytes, $t_{(54)} = 3.28$, $p$ = 0.000182, unpaired $t$ test). The duration ($T_{50}$) of EFS evoked responses was ~4 s in P2Y1OE and control slices (Fig. 2*E*; Control, 4.2 ± 0.5 s, $n$ = 13 astrocytes; P2Y1OE, 3.6 ± 0.3 s, $n$ = 42 astrocytes, $t_{(53)} = 0.83$, $p$ = 0.40817, two-sample $t$ test), suggesting that intracellular mechanisms downstream of P2Y1Rs were equivalent. EFS-evoked $Ca^{2+}$ signals were almost abolished by MRS 2179 (30 $\mu$M), a P2Y1R-specific antagonist, in both control and P2Y1OE slices (Fig. 2*E*,*F*; Before MRS 2179 for Control, 1.9 ± 0.4, During MRS 2179 for Control, 0.4 ± 0.2, $n$ = 58 astrocytes, $t_{(57)} = 3.48$, $p$ = 0.00096, paired $t$ test; Before MRS 2179 for P2Y1OE, 5.9 ± 0.6, During MRS 2179 for control, 0.09 ± 0.08, $n$ = 56 astrocytes, $t_{(57)} = 9.73$, $p = 1 \times 10^{-11}$, paired $t$ test). EFS-evoked $Ca^{2+}$ signals were also abolished by TTX (1 $\mu$M) in both control and P2Y1OE slices, indicating that a neuronal activity-dependent mechanism caused these signals (Fig. 2*G*; Before TTX for control, 0.73 ± 0.33, TTX for control, 0.05 ± 0.04, $n$ = 45 astrocytes from 3 slices, $t_{(44)} = 2.08$, $p$ = 0.04356, paired $t$ test; Before TTX for P2Y1OE, 4.2 ± 0.6, TTX for P2Y1OE, 0.26 ± 0.11, $n$ = 49 astrocytes from 4 slices, $t_{(48)} = 6.47$, $p = 5 \times 10^{-7}$, paired $t$ test). These data show that evoked $Ca^{2+}$ signals by endogenous ATP were also much larger in P2Y1OE astrocytes. Overall, EFS-evoked $Ca^{2+}$ signals suggest that P2Y1OE astrocytes express more functional P2Y1Rs than controls, which enable astrocytes to respond to endogenous ligands, once ATP is released via synaptic transmission.

### Occurrence of spontaneous microdomain $Ca^{2+}$ signals in processes were equivalent between control and P2Y1OE mice

Astrocytes display spatiotemporally distinct $Ca^{2+}$ signals, which have been reported both *in vitro* and *in vivo* through different mechanisms (Bazargani and Attwell, 2016; Shigetomi et al., 2016). Recent data from slice preparations and anesthetized animals show that the vast majority of $Ca^{2+}$ signals occur locally (Shigetomi et al., 2013; Gee et al., 2014; Haustein et al., 2014;

Kanemaru et al., 2014; Wu et al., 2014; Jiang et al., 2016; Rungta et al., 2016; Stobart, 2018). We focused on the ML of the DG, because ~90% of synapses are ensheathed by astrocyte processes in the ML (Bosch et al., 2016) and local application of a P2Y1 agonist causes microdomain (~4 $\mu$m) $Ca^{2+}$ signals at astrocyte processes, and P2Y1 activation via endogenous ligand mediates such microdomain $Ca^{2+}$ signals in young mice (Di Castro et al., 2011). We therefore tested whether astrocytes overexpressing P2Y1Rs show more microdomain (i.e., local) $Ca^{2+}$ signals or spatially expanded $Ca^{2+}$ signals. We took images at one frame per second for 5 min at high magnification, which captured two or three astrocytes. In both Control and P2Y1OE slices, we observed numerous local $Ca^{2+}$ signals that were similar in size to microdomain $Ca^{2+}$ signals (Movies 1, 2). First, we drew ROIs at processes and looked at the $Ca^{2+}$ dynamics (Fig. 3*A*). The frequency of $Ca^{2+}$ signals was not significantly different between control and P2Y1OE mice (Fig. 3*C*; Control, 6.9 ± 0.53 events per 5 min, $n = 79$ ROIs; P2Y1OE, 7.9 ± 0.56 events per 5 min, $n = 99$ ROIs, $t_{(176)} = 1.17$, $p = 0.24420$, unpaired $t$ test). There was no significant difference in dF/F (Fig. 3*D*; Control, 0.58 ± 0.02, $n = 549$ events; P2Y1OE, 0.57 ± 0.01, $n = 725$ events, $t_{(1272)} = 0.559$, $p = 0.5762$, unpaired $t$ test). The $T_{50}$ of microdomain $Ca^{2+}$ signals was slightly shorter in P2Y1OE mice (Fig. 3*E*; Control, 2.2 ± 0.06 s, $n = 549$ events; P2Y1OE, 1.9 ± 0.05 s, $n = 725$ events, $t_{(1272)} = 4.22$, $p = 0.000027$, unpaired $t$ test). Although the kinetics of microdomain $Ca^{2+}$ events were significantly shorter by ~10%, the overall number of microdomain $Ca^{2+}$ signals were equivalent.

ROI-based analysis is very useful for the quantification of $Ca^{2+}$ signals in astrocytes (Shigetomi et al., 2013; Srinivasan et al., 2015). However, there is huge spatial variation of signals. Even at the same location, the area showing microdomain $Ca^{2+}$ signals varied with time (Fig. 3*F*; Movies 1, 2). Conventional methods based on ROIs do not provide information on spatial dynamics of microdomain $Ca^{2+}$ signals. To quantify spatial information, we simply picked up all fluorescence increases above the threshold (see Materials and Methods) and analyzed the area of $Ca^{2+}$ signals that were >1 $\mu m^2$. In this way, we were able to analyze $Ca^{2+}$ signals without bias. Typical FOV areas were 25931.69 $\mu m^2$. The number of areas displaying $Ca^{2+}$ signals in P2Y1OE and control astrocytes was equivalent (Control

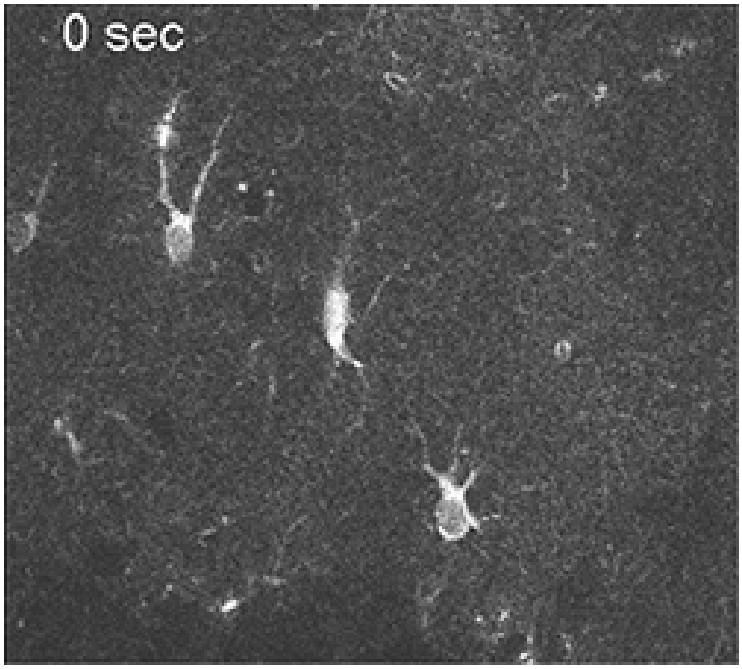


**Movie 1.** Representative video of $Ca^{2+}$ signals in astrocytes from control mice. Most signals occurred locally.

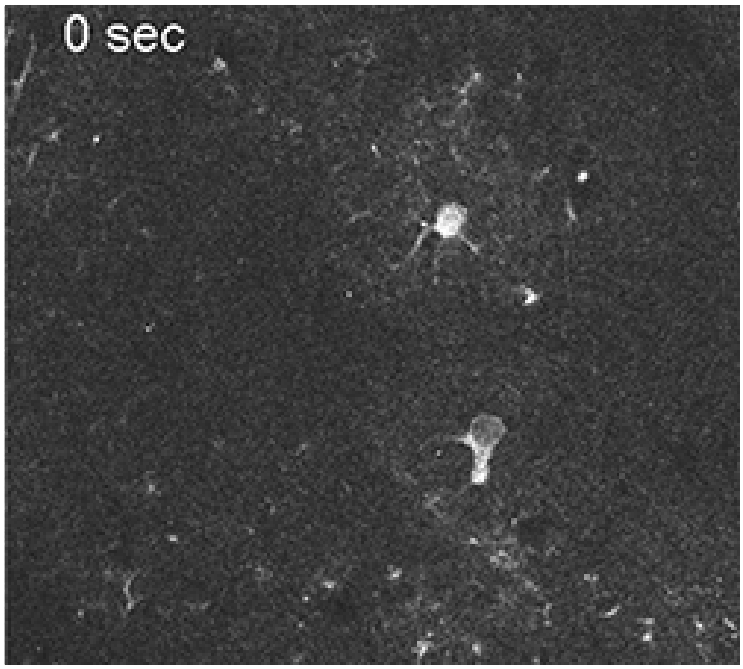


**Movie 2.** Representative video of $Ca^{2+}$ signals in astrocytes from P2Y1OE mice. Many signals occurred locally. Occasionally, $Ca^{2+}$ waves were seen.

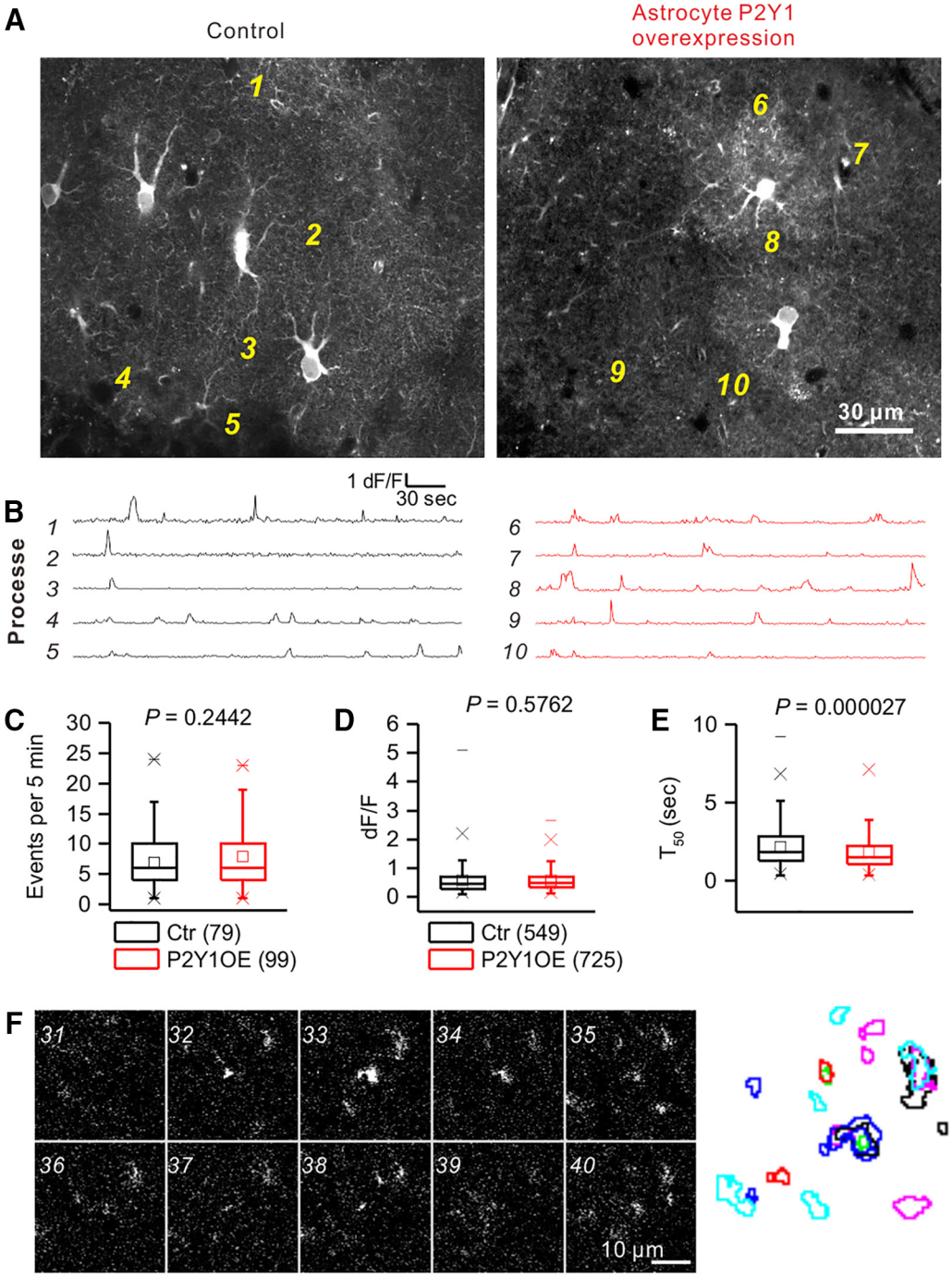


**Figure 3.** Microdomain $Ca^{2+}$ signals in astrocytes. ***A***, Representative F images of astrocytes expressing GCaMP6f. ***B***, Traces were taken from the ROIs as indicated in ***A***. Many $Ca^{2+}$ signals were observed both in control and P2Y10E astrocytes. ***C***, Summary of event frequency of $Ca^{2+}$ signals. ***D***, Summary of peak dF/F of spontaneous $Ca^{2+}$ signals. ***E***, Summary of duration of $T_{50}$ of spontaneous $Ca^{2+}$ signal. No obvious difference was observed in P2Y10E astrocytes compared with controls. ***F***, Sequential dF images of part of an FOV. Top left, The number indicates the time of images taken. Right, The result of "particle analysis" of microdomain $Ca^{2+}$ signals. The area and the position of $Ca^{2+}$ signals were variable, suggesting that the conventional ROI method to analyze $Ca^{2+}$ signals was not appropriate for spontaneous microdomain $Ca^{2+}$ signals occurring locally.

9650 ± 1780 areas from 10 FOVs from 5 slices; P2Y1OE, 9810 ± 1490 areas from 13 FOVs from 9 slices, $t_{(21)} = 0.0705$, $p = 0.9445$, unpaired $t$ test). The size of the vast majority (70%–80%) of $Ca^{2+}$ signals was $<4\ \mu m^2$ (Fig. 4*C*). However, the size distribution was different (Fig. 4*B*,*C*). When we plotted the areas versus dF/F, large events in terms of area appeared in P2Y1OE astrocytes that were not observed in controls (Fig. 4*B*). The cumulative distribution of areas was significantly different between control and P2Y1OE astrocytes (Fig. 4*C*; Control, $n = 10$ FOVs; P2Y1OE, $n = 13$ FOVs, $D = 0.22826$, $p = 0.000019$, Kolmogorov–Smirnov test). The two distribution curves crossed ~43 $\mu m^2$ (Fig. 4*C*). Because of the difference in $Ca^{2+}$ signals in terms of area, we simply calculated the number of microdomain $Ca^{2+}$ events. The number of areas $<3\ \mu m^2$ in astrocytes were equivalent (Fig. 4*F*; Control, 4490 ± 803 areas from 10 FOVs; P2Y1OE, 5040 ± 720 areas from 13 FOVs, $t_{(21)} = 0.5079$, $p = 0.61683$, unpaired $t$ test). Similar results were obtained for areas $<12\ \mu m^2$ (Fig. 4*F*; Control, 8000 ± 1480 areas; P2Y1OE, 8650 ± 1310 areas, $t_{(21)} = 0.3291$, $p = 0.74537$, unpaired $t$

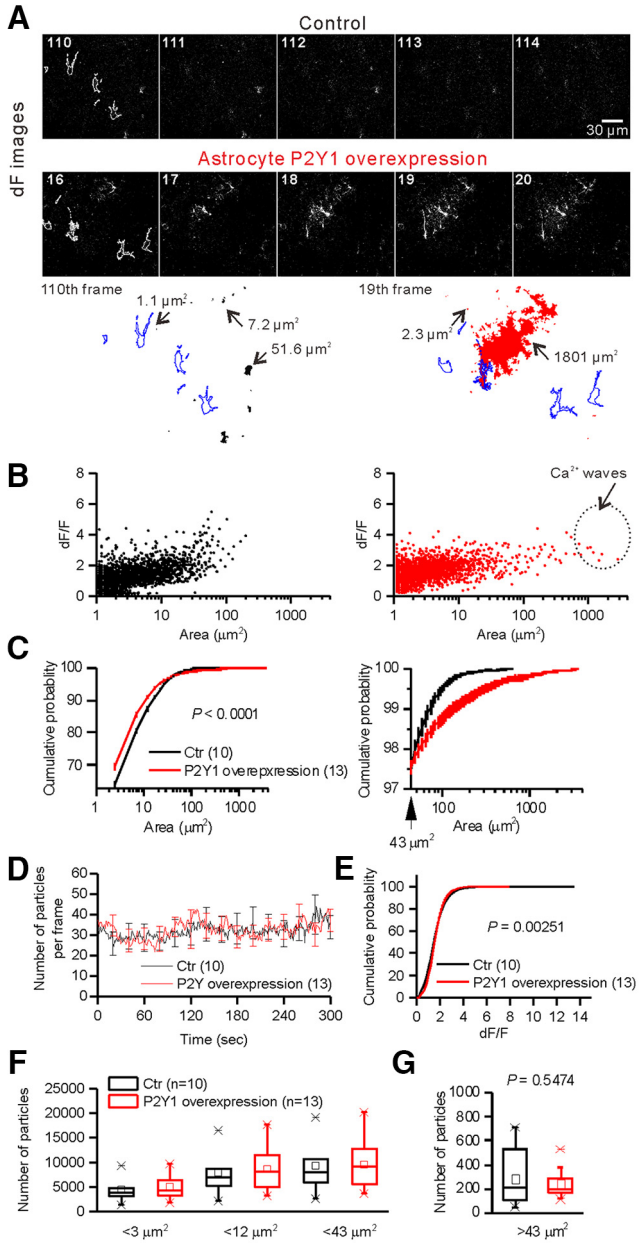


**Figure 4.** Equivalent numbers of $Ca^{2+}$ signals were observed in control and P2Y10E astrocytes. ***A***, Representative images of dF. White lines in the images indicate the outlines of astrocytes. Objects below the images are representative $Ca^{2+}$ signals. Perimeters were drawn. The numbers beside the objects indicate the area showing $Ca^{2+}$ signals. There are multiple $Ca^{2+}$ signals found in the same FOV. The largest object in P2Y10E represents $Ca^{2+}$ waves. Blue lines indicate the outlines of astrocytes. ***B***, Relationship between the area and dF/F of spontaneous $Ca^{2+}$ signals. P2Y10E astrocytes showed larger $Ca^{2+}$ signals (>700 $\mu m^2$) in terms of area not observed in control. Such events were called "$Ca^{2+}$ waves." ***C***, Cumulative probability plot of the area. Two lines crossed at 43 $\mu m^2$. Traces for signals >43 $\mu m^2$ are shown in the right-hand graph. ***D***, Summary of the number of $Ca^{2+}$ signals in each frame. No difference in the number of $Ca^{2+}$ signals was observed between control and P2Y10E astrocytes. ***E***, Cumulative probability of dF/F. The distribution of dF/F was significantly affected by overexpression of P2Y1 receptors ($D = 0.25147$, $p = 0.00251$, Kolmogorov–Smirnov test). ***F***, Summary of the number of areas in each FOV. There was no significant difference between control and P2Y10E astrocytes. ***G***, Summary of the number of large (>43 $\mu m^2$) areas in each FOV.

test) and 43 $\mu m^2$ (Fig. 4*F*; Control, 9330 ± 1740 areas; P2Y1OE, 9570 ± 1470 areas, $t_{(21)} = 0.10574$, $p = 0.91679$, unpaired *t* test). Large (>43 $\mu m^2$) signal areas were also equivalent (Fig. 4*G*; Control, 288 ± 73 areas; P2Y1OE, 243 ± 32 areas, $t_{(21)} = 0.6115$, $p = 0.54743$, unpaired *t* test). Overall, these data suggest that the number of microdomain $Ca^{2+}$ events was not increased by overexpression of P2Y1R in astrocytes.

### Microdomain $Ca^{2+}$ signals in P2Y1OE astrocytes were not reduced by P2Y1R blockade

We did not observe an increase in the number of microdomain $Ca^{2+}$ signals by overexpression of P2Y1Rs. However, it is possible that microdomain $Ca^{2+}$ signals are indeed P2Y1R-dependent but that the total number of microdomain $Ca^{2+}$ signals did not change because of a compensatory mechanism. However, this was not the case because MRS 2179 (30 $\mu$M), a P2Y1R-specific antagonist, did not affect the number of microdomain $Ca^{2+}$ signals (Fig. 5). The number of areas <3 $\mu m^2$ were equivalent (Control, 4870 ± 1020 areas; P2Y1OE, 4100 ± 1240 areas, $n = 7$ FOVs, $t_{(6)} = 1.023$, $p = 0.34557$, paired *t* test) and similar results were obtained for <12 $\mu m^2$ (Control, 8690 ± 1750 areas; P2Y1OE, 7150 ± 2360 areas, $n = 7$ FOVs, $t_{(6)} = 1.564$, $p = 0.18331$, paired *t* test) and < 43 $\mu m^2$ areas (Control, 9700 ± 2030 areas; P2Y1OE, 7940 ± 2720 areas, $n = 7$ FOVs, $t_{(6)} = 1.515$, $p = 0.18049$, paired *t* test). These data indicate that small-size local events are P2Y1R-independent, indicating that microdomain $Ca^{2+}$ events do not occur through the activation of P2Y1Rs in acute brain slices of mice.

### $Ca^{2+}$ waves in P2Y1OE astrocytes

Overexpression of P2Y1Rs in astrocytes enlarged $Ca^{2+}$ signals without affecting the number of $Ca^{2+}$ signals observed, indicating that global rather than local signals are mediated by the activation of P2Y1Rs. This indicates that ATP is released onto astrocytes without any stimulus. MRS 2179 selectively inhibited the events >43 $\mu m^2$ (Control, 267 ± 54 areas; P2Y1OE, 101 ± 62 areas, $n = 7$ FOVs, $t_{(6)} = 4.668$, $p = 0.00344$, paired *t* test; Fig. 5*E*). $Ca^{2+}$ signals that spread to areas of >700 $\mu m^2$ were only observed in P2Y1OE astrocytes after imaging for 5 min (Figs. 4–6) and such wide-spreading $Ca^{2+}$ signals were completely abolished in the presence of MRS 2179 (Fig. 5*A*). These events were fully recovered after washout of MRS 2179 for 5 min (data not shown), suggesting that the activation of P2Y1Rs by endogenous ligands caused these large $Ca^{2+}$ events. $Ca^{2+}$ spreading events were 1.9-fold larger than microdomain $Ca^{2+}$ signals (Fig. 4*B*; <43 $\mu m^2$, 1.7 ± 0.1; > 700 $\mu m^2$, 3.3 ± 0.3, $n = 12$ FOVs, $t_{(11)} = 7.918$, $p = 0.000007$, paired *t* test). The duration of the $Ca^{2+}$ signals was 2.9-fold longer than that of microdomain $Ca^{2+}$ signals (microdomain $Ca^{2+}$ signal, 1.9 ± 0.1 s; $Ca^{2+}$ wave, 5.5 ± 0.8 s, $t_{(778)} = 12.56$, $p = 4 \times 10^{-33}$, unpaired *t* test). A total of 19 ± 2% of $Ca^{2+}$ waves started in main branches. A total of 36 ± 4% of $Ca^{2+}$ waves started in fine processes. A total of 9 ± 3% of $Ca^{2+}$ waves started in endfeet. Only 2 ± 2% of $Ca^{2+}$ waves started in soma. The initial sites of the remaining $Ca^{2+}$ waves (33 ± 4%) were difficult to be determined due to the fairly large area of initial events. The majority of the $Ca^{2+}$ signals whose initial sites were identified started in processes and spread throughout the astrocytes. $Ca^{2+}$ spreading events accounted for only 2% of total $Ca^{2+}$ signal events (Fig. 4*B*) but spread to areas of up to ~3600 $\mu m^2$, which is 80-fold larger than the majority (98%) of events. In many cases, $Ca^{2+}$ signals spread into neighboring astrocyte territories (Fig. 4*A*; Movie 2). These signals traveled at 17 ± 3 $\mu$m/s initially and then slowed to 4.1 ± 0.6 $\mu$m at 30 $\mu$m from the initiation site (Fig. 6*B*,*C*), indicating that diffusion of the ligand determined how far the $Ca^{2+}$ signal spread. Consistent with this, the dF/F peak decreased with distance from the initial $Ca^{2+}$ signal site (Fig. 6*B*). Based on the characteristics of the $Ca^{2+}$ signals, we named them "$Ca^{2+}$ waves."

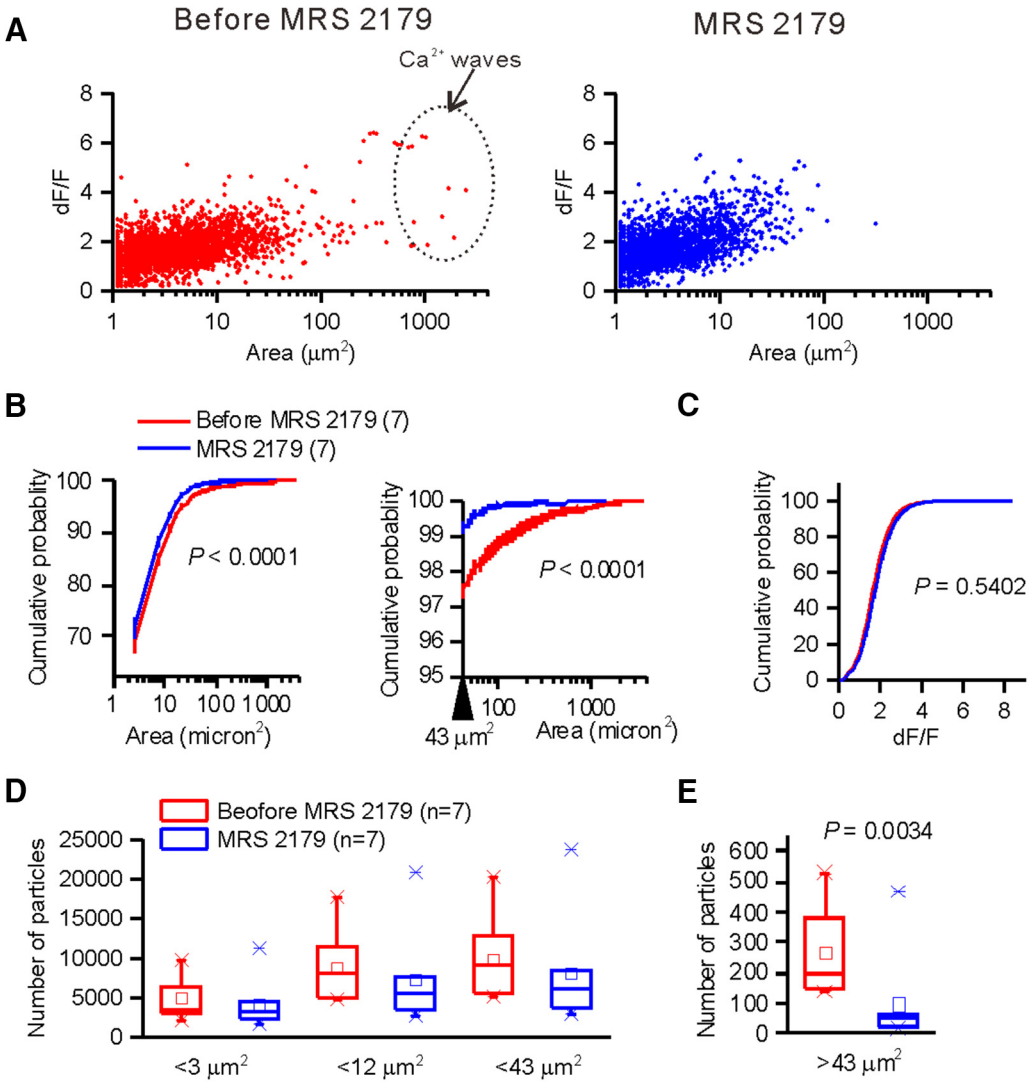


**Figure 5.** MRS 2179 selectively reduced $Ca^{2+}$ waves observed in P2Y1OE astrocytes. ***A***, The relationship between the area and dF/F. Dashed circles represent $Ca^{2+}$ waves. Such $Ca^{2+}$ waves disappeared in the presence of MRS 2179 (30 $\mu$M, right). ***B***, Cumulative probability plot of the area displaying $Ca^{2+}$ signals. MRS 2179 affected the distribution of areas ($D = 0.3097$, $p = 1.8 \times 10^{-17}$, Kolmogorov–Smirnov test). ***C***, Cumulative probability of dF/F. MRS 2179 (30 $\mu$M) did not affect the dF/F ($D = 0.12024$, $p = 0.76967$, Kolmogorov–Smirnov test). ***D***, Summary of the areas with or without MRS 2179. ***E***, Summary of the area of large (>43 $\mu m^2$) $Ca^{2+}$ events. MRS 2179 significantly reduced the number of large $Ca^{2+}$ events.

### Pharmacological properties of $Ca^{2+}$ waves in P2Y1OE astrocytes

Next, we asked how $Ca^{2+}$ waves occur. We imaged larger FOVs to image many astrocytes simultaneously and focused only on areas of >700 $\mu m^2$. The average number of areas of >700 $\mu m^2$ that occurred in 5 min in an area of 10,000 $\mu m^2$ was 145 ± 15 ($n = 24$ FOVs, 11–312 waves). There were preferential sites where $Ca^{2+}$ waves started (Fig. 6*D*). Generally, $Ca^{2+}$ waves propagated radially. There was no obvious orientation in which $Ca^{2+}$ waves preferentially propagated. Application of TTX (1 $\mu$M for 10 min) to inhibit action potentials did not affect the event number (Fig. 6*D–F*; Control, 112 ± 27 waves; TTX, 114 ± 34 waves, $n = 7$ slices, $t_{(6)} = 0.1332$, $p = 0.89841$, paired $t$ test), suggesting that $Ca^{2+}$ waves do not result from action-potential-dependent neurotransmitter release. In the CNS, both neurons and glial cells are able to release ATP. Various pathways for ATP release have been proposed, such as exocytosis, and release through ion channels and transporters (Fields and Burnstock, 2006; Koizumi, 2010). Channel-mediated pathways are well characterized; therefore, we analyzed them pharmacologically. To inhibit the connexin/pannexin channel-mediated pathway, we applied CBX (100 $\mu$M for 10 min). CBX decreased the number of events slightly but not significantly (Fig. 6*G*; Control, 151 ± 21 waves; CBX, 110 ± 22 waves, $n = 8$ slices, $t_{(7)} = 2.176$, $p = 0.06604$, paired $t$ test). Probenecid (PB) inhibits the pannexin channel and the organic anion transporter (Silverman et al., 2009). PB (5 mM for 10 min) significantly reduced the event number (Fig. 6*H*; Control, 177 ± 36 waves; PB, 26 ± 11 waves, $n = 5$ slices, $t_{(4)} = 5.346$, $p = 0.0059$, paired $t$ test). Although PB reduced the occurrence of $Ca^{2+}$ waves, high concentrations (5 mM) were required, indicating that pannexin may not contribute to ATP release for the $Ca^{2+}$ waves. Brilliant blue G did not affect the frequency of $Ca^{2+}$ waves (data not shown), indicating that the P2X7 receptor is unlikely to contribute to $Ca^{2+}$ wave generation. Cyclopiazonic acid (CPA, 20 $\mu$M, 10 min) completely abolished the events (Fig. 6*I*; Control, 154 ± 50 waves, CPA, 0 ± 0 wave, $n = 4$ slices, $U = 16$, $p = 0.02107$, Mann–Whitney test), suggesting that $Ca^{2+}$ release from intracellular $Ca^{2+}$ stores is the main intracellular mechanism for $Ca^{2+}$ waves. This is consistent with the idea that Gq-protein coupled P2Y1R mediated the $Ca^{2+}$ waves. Overall, our data in-

dicate that $Ca^{2+}$ waves result from ATP release through a PB-sensitive pathway.

## Discussion

Astrocyte processes produce numerous microdomain $Ca^{2+}$ signals that occur spontaneously. It has been suggested that local synaptic transmission elicits microdomain-like local $Ca^{2+}$ signals in astrocytes via GqPCR activation (Jourdain et al., 2007; Di Castro et al., 2011; Panatier et al., 2011); however, it is not clear whether microdomain $Ca^{2+}$ signals that spontaneously occur at astrocyte processes are due to local synaptic transmission because spontaneous $Ca^{2+}$ signals are insensitive to GqPCR antagonists (Nett et al., 2002; Haustein et al., 2014). To ask whether microdomain $Ca^{2+}$ signals are due to GqPCR activation, we manipulated gene expression of a major GqPCR, the P2Y1R, specifically in astrocytes. By monitoring $Ca^{2+}$ signals in astrocytes using a GECI, we found larger responses to exogenously applied ligand and repetitive electrical stimulation of axons in astrocytes overexpressing P2Y1Rs (Fig. 2). However, no obvious changes in the number and dF/F of microdomain $Ca^{2+}$ signals were observed, although GECI identified numerous microdomain $Ca^{2+}$ signals in astrocytes (Figs. 3–5). Instead, we observed spatially widespread $Ca^{2+}$ signals, $Ca^{2+}$ waves, which accounted for only 2% of total $Ca^{2+}$ events but that were significantly larger and longer than microdomain $Ca^{2+}$ signals at processes. Our data indicate that the P2Y1R plays a role in $Ca^{2+}$ signals in the DG but does not contribute to spontaneously occurring microdomain $Ca^{2+}$ signals in astrocytes.

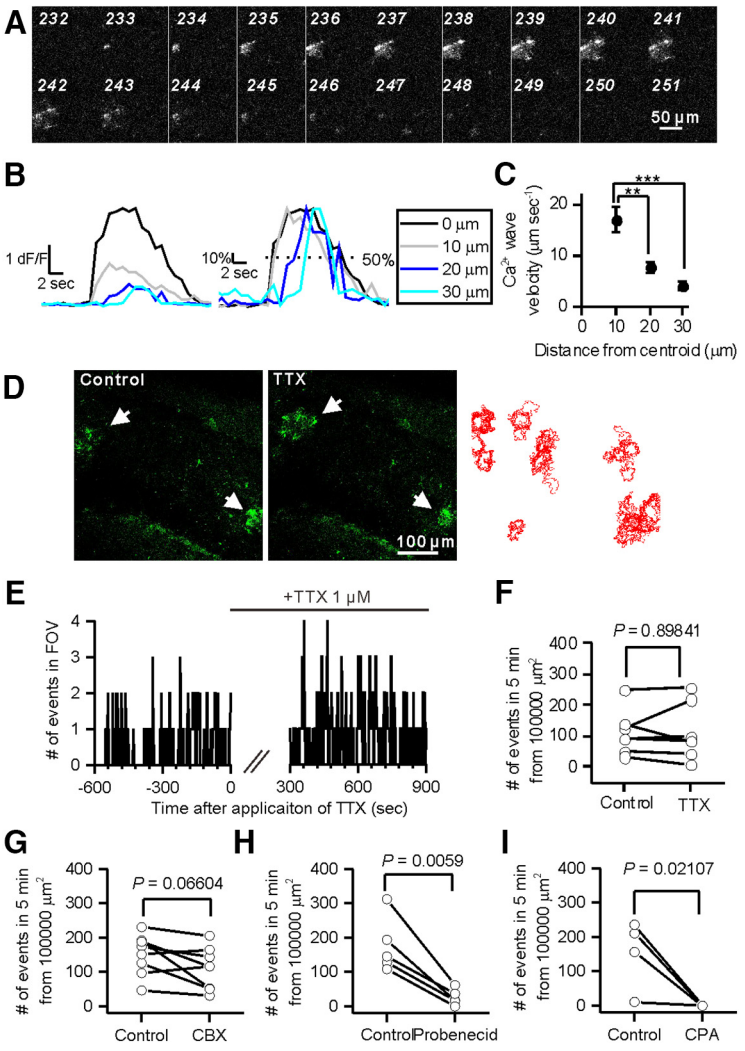


**Figure 6.** $Ca^{2+}$ waves occurred via a PB-sensitive pathway. ***A***, Montage of sequential images of $Ca^{2+}$ waves. ***B***, Left, Representative traces of intensity versus time profiles of $Ca^{2+}$ waves. Right, Normalized traces of the left traces. Dotted line indicates 50% of the peak. ***C***, Velocity of $Ca^{2+}$ waves. The velocity declined away from the initial site (0 $\mu$m): 10 $\mu$m, 17 $\pm$ 2.6 $\mu$m/s; 20 $\mu$m, 7.7 $\pm$ 1.1 $\mu$m/s; 30 $\mu$m, 4.1 $\pm$ 0.6 $\mu$m/s. Comparison between 10 and 20 $\mu$m; $t_{(19)} = 3.697$, $p = 0.00153$. Comparison between 10 and 30 $\mu$m; $t_{(19)} = 5.616$, $p = 0.00002$. ***D***, $Ca^{2+}$ waves were observed both before and in the presence of TTX (1 $\mu$M). Arrows indicate $Ca^{2+}$ waves. Such events generally occurred at similar locations. Right, Overlay of the perimeter of each $Ca^{2+}$ wave observed in 5 min. ***E***, Representative trace of the number of $Ca^{2+}$ waves. TTX was applied during the period indicated by a bar. ***F***, Summary of the effect of TTX on $Ca^{2+}$ waves. ***G***, Summary of the effect of CBX (100 $\mu$M) on $Ca^{2+}$ waves. ***H***, Summary of the effect of PB (5 mM) on $Ca^{2+}$ waves. ***I***, Summary of the effect of CPA (20 $\mu$M) on $Ca^{2+}$ waves. $^{**}p < 0.01$. $^{***}p < 0.0001$.

### Monitoring extracellular ATP via astrocyte-specific overexpression of functional P2Y1Rs

Extracellular ATP acts as a neuromodulator and is released through multiple pathways from multiple cell types in the CNS (Fields and Burnstock, 2006). However, the spatiotemporal release of ATP is poorly understood because of a lack of methodology to monitor its spatiotemporal dynamics. In this study, by monitoring $Ca^{2+}$ signals in entire astrocyte territories from transgenic mice that specifically overexpress P2Y1Rs (Tanaka et al., 2010), we successfully detected the endogenous ligand for the P2Y1R, most likely ATP. Both exogenous and endogenous ligands induced significantly larger (twofold to threefold) $Ca^{2+}$ signals in P2Y1OE astrocytes compared with control astrocytes. P2Y1R-agonist evoked responses initially started at processes in ~85% of astrocytes, indicating the expression of functional P2Y1Rs at astrocyte processes. In addition, $Ca^{2+}$ waves observed in P2Y1OE astrocytes initially started in processes in most of cases. Although our ISH data do not show subcellular localization of P2Y1Rs in P2Y1OE astrocytes, our functional analysis showed that the centroid of $Ca^{2+}$ waves initiated at both fine processes (~36%) and main branches (19%). If P2Y1Rs are increased only in main branches in P2Y1OE, this may cause more frequent local $Ca^{2+}$ signals in the main branches, but our data do not support this. Thus, we think that P2Y1Rs would be expressed evenly in plasma membrane of astrocytes, including on the membrane of astrocyte processes to detect locally released ATP, but we must await further studies to clarify its subcellular localization.

Evoked $Ca^{2+}$ signals by perforant path stimulation were blocked by TTX. Therefore, these signals were due to action-potential-dependent release of ATP most likely from the axon termini. Because ~88% of responses were reduced by MRS 2179, a P2Y1R specific antagonist, the P2Y1R is the major GqPCR receptor in adult DG astrocytes to receive neuronal information, which is consistent with a previous observation (Jourdain et al., 2007).

### Microdomain $Ca^{2+}$ signals observed in P2Y1OE astrocytes

Using AAV-mediated introduction of GECI into astrocytes, we observed numerous $Ca^{2+}$ signals at astrocyte processes, which are difficult to visualize by conventional bulk loading of organic $Ca^{2+}$ indicator (Reeves et al., 2011). The expression level of GFAP after introduction of GCaMP6f was comparable between control and P2Y1OE astrocytes (Fig. 1*C*,*D*), suggesting that imaging conditions were similar for control and P2Y1OE cells, although there is a concern that overexpression of GECI may affect astrocyte physiology (Ortinski et al., 2010).

The P2Y1R mediates local $Ca^{2+}$ signals at astrocyte processes in the ML of the DG (Di Castro et al., 2011; Santello et al., 2011). The P2Y1R is also known to be expressed in neurons; therefore, we took a transgenic approach to manipulate *P2ry1* expression specifically in astrocytes. We then asked whether astrocytes overexpressing P2Y1Rs show increased numbers of microdomain $Ca^{2+}$ signals in astrocytes in the ML of the DG. However, we did not find an increase in either the dF/F or the number of microdomain $Ca^{2+}$ signals in P2Y1OE astrocytes. The simplest explanation for this result is that P2Y1Rs may not contribute to the vast majority of microdomain $Ca^{2+}$ signals in our preparations. Although our functional evidence indicates that P2Y1Rs are localized evenly in astrocytes, as mentioned above, P2Y1Rs may not exist at the point source of ATP release. It is possible that other GqPCRs exist and contribute to IP3 receptor-mediated microdomain $Ca^{2+}$ signals in processes where P2Y1Rs are not located. Differences in methods used to measure microdomain $Ca^{2+}$ signals may lead to different results (i.e., pipette loading of Fluo-4 vs AAV-mediated GECI). However, comparison between pipette loading of Fluo-4 and virally expressed GCaMP3 indicates that both methods produce similar microdomain $Ca^{2+}$ signals (Rungta et al., 2016).

Our data on microdomain $Ca^{2+}$ signals at astrocyte processes in the DG are consistent with a recent observation of $Ca^{2+}$ signals at astrocyte processes of mice not being mediated by GqPCRs (Haustein et al., 2014; Jiang et al., 2016; Rungta et al., 2016). Recently, Agarwal et al. (2017) showed that $Ca^{2+}$ efflux through permeability transition pores in mitochondria is responsible for microdomain $Ca^{2+}$ signals in mice *in vivo*. This mitochondrial $Ca^{2+}$ release seems to be independent of synaptic transmission. Induction of GqPCR-mediated $Ca^{2+}$ signals at astrocyte processes probably requires repetitive stimuli (Haustein et al., 2014; Tang et al., 2015; Jiang et al., 2016; Stobart, 2018). We performed 2D imaging; therefore, we may have missed spontaneous microdomain $Ca^{2+}$ signals elicited by minimal neuronal activities. These may be apparent using 3D imaging techniques (Bindocci et al., 2017).

### $Ca^{2+}$ waves in P2Y1OE astrocytes

The P2Y1R-mediated $Ca^{2+}$ waves observed in P2Y1OE mice indicates that the combination of P2Y1R overexpression and $Ca^{2+}$ imaging by GECI successfully enabled the release of endogenous ligand for P2Y1R onto astrocytes to be monitored. We found that $Ca^{2+}$ waves occurred through a PB-sensitive mechanism, indicating that the ABC transporter or anion channels contribute to the release of ATP for $Ca^{2+}$ waves (Koizumi, 2010). However, we do not exclude the possibility that vesicular release of ATP contributes to $Ca^{2+}$ waves. Subtle release of ATP may trigger more release of ATP to lead to $Ca^{2+}$ waves (Anderson et al., 2004). ATP can be released from various cell types through various mechanisms; therefore, it is difficult to elucidate the source of ATP without knowing the exact mechanism underlying ATP release.

$Ca^{2+}$ waves in P2Y1OE astrocytes resembled glial $Ca^{2+}$ waves observed in the cerebellum *in vivo* (Hoogland et al., 2009; Nimmerjahn et al., 2009; Mathiesen et al., 2013), in the retina *in situ* (Kurth-Nelson et al., 2009), and in the cortex of Alzheimer disease model mice *in vivo* (Delekate et al., 2014) because these glial waves spread at a similar rate and occur through P2 receptor activation independently of action potentials. Mathiesen et al. (2013) show that ATP-evoked glial $Ca^{2+}$ waves reduce tissue oxygen tension in the cerebellum, suggesting that glial waves increase oxygen consumption. Reduced oxygen tension could be caused by increased neuronal activities or reduced oxygen supply from the blood. Such $Ca^{2+}$ waves may contribute to neuronal functions because P2Y1R-mediated signals contribute to gliotransmitter release to enhance excitatory and inhibitory synaptic transmission (Bowser and Khakh, 2004; Pascual et al., 2012; Álvarez-Ferradas et al., 2015; Tan et al., 2017) and neurotransmitter uptake (Jacob et al., 2014). Experiments using two-color imaging of both astrocytes and neurons may elucidate whether and how $Ca^{2+}$ waves regulate neuronal activities (Brancaccio et al., 2017).

### Pathophysiological significance of astrocyte-specific P2Y1R overexpression

The P2Y1R can be upregulated in astrocytes in pathophysiological states (Kuboyama et al., 2011; Delekate et al., 2014) and contributes to $Ca^{2+}$ signals, for example, in Alzheimer disease (Delekate et al., 2014) and epilepsy (Álvarez-Ferradas et al., 2015). Our data indicate that increased expression of P2Y1Rs in astrocytes contributes to $Ca^{2+}$ waves but not to microdomain $Ca^{2+}$ signals. It seems that the augmentation of P2Y1R-mediated signals in astrocytes in pathophysiological sates contributes to global changes in the neuronal network or vascular regulation rather than the local regulation of synaptic transmission (Araque et al., 2014). A single astrocyte is able to modulate >100,000 synapses in its territory (Bushong et al., 2002) and $Ca^{2+}$ waves propagate to large areas; therefore, P2Y1R-mediated $Ca^{2+}$ waves may activate many synapses simultaneously, which may cause aberrant activities in neuronal networks, as observed in Alzheimer disease models and epilepsy (Koizumi, 2010; Rassendren and Audinat, 2016). In pathophysiological states, the expression of many genes is altered in addition to the P2Y1R (Burda and Sofroniew, 2014). Our transgenic mice may help to understand the specific role of P2Y1R-mediated $Ca^{2+}$ signals in neuronal network excitability. Our findings on $Ca^{2+}$ signals in astrocytes overexpressing one GqPCR may also have important implications for the function and role of $Ca^{2+}$ signals in astrocytes, especially in pathophysiological states (Delekate et al., 2014; Kim et al., 2016).

## References

Agarwal A, Wu PH, Hughes EG, Fukaya M, Tischfield MA, Langseth AJ, Wirtz D, Bergles DE (2017) Transient opening of the mitochondrial permeability transition pore induces microdomain calcium transients in astrocyte processes. Neuron 93:587–605.e7. CrossRef Medline

Agulhon C, Petravicz J, McMullen AB, Sweger EJ, Minton SK, Taves SR, Casper KB, Fiacco TA, McCarthy KD (2008) What is the role of astrocyte calcium in neurophysiology? Neuron 59:932–946. CrossRef Medline

Álvarez-Ferradas C, Morales JC, Wellmann M, Nualart F, Roncagliolo M, Fuenzalida M, Bonansco C (2015) Enhanced astroglial $Ca^{2+}$ signaling increases excitatory synaptic strength in the epileptic brain. Glia 63:1507–1521. CrossRef Medline

Anderson CM, Bergher JP, Swanson RA (2004) ATP-induced ATP release from astrocytes. J Neurochem 88:246–256. CrossRef Medline

Araque A, Carmignoto G, Haydon PG, Oliet SH, Robitaille R, Volterra A (2014) Gliotransmitters travel in time and space. Neuron 81:728–739. CrossRef Medline

Bazargani N, Attwell D (2016) Astrocyte calcium signaling: the third wave. Nat Neurosci 19:182–189. CrossRef Medline

Bindocci E, Savtchouk I, Liaudet N, Becker D, Carriero G, Volterra A (2017) Three-dimensional $Ca^{2+}$ imaging advances understanding of astrocyte biology. Science 356:eaai8185. CrossRef Medline

Bosch C, Masachs N, Exposito-Alonso D, Martínez A, Teixeira CM, Fernaud I, Pujadas L, Ulloa F, Comella JX, DeFelipe J, Merchán-Perez A, Soriano E (2016) Reelin regulates the maturation of dendritic spines, synaptogenesis and glial ensheathment of newborn granule cells. Cereb Cortex 26: 4282–4298. CrossRef Medline

Bowser DN, Khakh BS (2004) ATP excites interneurons and astrocytes to increase synaptic inhibition in neuronal networks. J Neurosci 24:8606–8620. CrossRef Medline

Brancaccio M, Patton AP, Chesham JE, Maywood ES, Hastings MH (2017) Astrocytes control circadian timekeeping in the suprachiasmatic nucleus via glutamatergic signaling. Neuron 93:1420–1435.e5. CrossRef Medline

Burda JE, Sofroniew MV (2014) Reactive gliosis and the multicellular response to CNS damage and disease. Neuron 81:229–248. CrossRef Medline

Bushong EA, Martone ME, Jones YZ, Ellisman MH (2002) Protoplasmic astrocytes in CA1 stratum radiatum occupy separate anatomical domains. J Neurosci 22:183–192. Medline

Chen TW, Wardill TJ, Sun Y, Pulver SR, Renninger SL, Baohan A, Schreiter ER, Kerr RA, Orger MB, Jayaraman V, Looger LL, Svoboda K, Kim DS (2013) Ultrasensitive fluorescent proteins for imaging neuronal activity. Nature 499:295–300. CrossRef Medline

Delekate A, Füchtemeier M, Schumacher T, Ulbrich C, Foddis M, Petzold GC (2014) Metabotropic P2Y1 receptor signalling mediates astrocytic hyperactivity in vivo in an Alzheimer's disease mouse model. Nat Commun 5:5422. CrossRef Medline

Di Castro MA, Chuquet J, Liaudet N, Bhaukaurally K, Santello M, Bouvier D, Tiret P, Volterra A (2011) Local $Ca^{2+}$ detection and modulation of synaptic release by astrocytes. Nat Neurosci 14:1276–1284. CrossRef Medline

Ding F, O'Donnell J, Thrane AS, Zeppenfeld D, Kang H, Xie L, Wang F, Nedergaard M (2013) α1-Adrenergic receptors mediate coordinated $Ca^{2+}$ signaling of cortical astrocytes in awake, behaving mice. Cell Calcium 54:387–394. CrossRef Medline

Fields RD, Burnstock G (2006) Purinergic signalling in neuron-glia interactions. Nat Rev Neurosci 7:423–436. CrossRef Medline

Gee JM, Smith NA, Fernandez FR, Economo MN, Brunert D, Rothermel M, Morris SC, Talbot A, Palumbos S, Ichida JM, Shepherd JD, West PJ, Wachowiak M, Capecchi MR, Wilcox KS, White JA, Tvrdik P (2014) Imaging activity in neurons and glia with a Polr2a-based and cre-dependent GCaMP5G-IRES-tdTomato reporter mouse. Neuron 83:1058–1072. CrossRef Medline

Haustein MD, Kracun S, Lu XH, Shih T, Jackson-Weaver O, Tong X, Xu J, Yang XW, O'Dell TJ, Marvin JS, Ellisman MH, Bushong EA, Looger LL, Khakh BS (2014) Conditions and constraints for astrocyte calcium signaling in the hippocampal mossy fiber pathway. Neuron 82:413–429. CrossRef Medline

Hoogland TM, Kuhn B, Göbel W, Huang W, Nakai J, Helmchen F, Flint J, Wang SS (2009) Radially expanding transglial calcium waves in the intact cerebellum. Proc Natl Acad Sci U S A 106:3496–3501. CrossRef Medline

Jacob PF, Vaz SH, Ribeiro JA, Sebastião AM (2014) P2Y1 receptor inhibits GABA transport through a calcium signalling-dependent mechanism in rat cortical astrocytes. Glia 62:1211–1226. CrossRef Medline

Jiang R, Diaz-Castro B, Looger LL, Khakh BS (2016) Dysfunctional calcium and glutamate signaling in striatal astrocytes from Huntington's disease model mice. J Neurosci 36:3453–3470. CrossRef Medline

Jourdain P, Bergersen LH, Bhaukaurally K, Bezzi P, Santello M, Domercq M, Matute C, Tonello F, Gundersen V, Volterra A (2007) Glutamate exocytosis from astrocytes controls synaptic strength. Nat Neurosci 10:331–339. CrossRef Medline

Kanemaru K, Sekiya H, Xu M, Satoh K, Kitajima N, Yoshida K, Okubo Y, Sasaki T, Moritoh S, Hasuwa H, Mimura M, Horikawa K, Matsui K, Nagai T, Iino M, Tanaka KF (2014) In vivo visualization of subtle, transient, and local activity of astrocytes using an ultrasensitive Ca(2+) indicator. Cell Rep 8:311–318. CrossRef Medline

Kawamura M, Gachet C, Inoue K, Kato F (2004) Direct excitation of inhibitory interneurons by extracellular ATP mediated by P2Y1 receptors in the hippocampal slice. J Neurosci 24:10835–10845. CrossRef Medline

Kim SK, Hayashi H, Ishikawa T, Shibata K, Shigetomi E, Shinozaki Y, Inada H, Roh SE, Kim SJ, Lee G, Bae H, Moorhouse AJ, Mikoshiba K, Fukazawa Y, Koizumi S, Nabekura J (2016) Cortical astrocytes rewire somatosensory cortical circuits for peripheral neuropathic pain. J Clin Invest 126: 1983–1997. CrossRef Medline

Koizumi S (2010) Synchronization of $Ca^{2+}$ oscillations: involvement of ATP release in astrocytes. FEBS J 277:286–292. CrossRef Medline

Kuboyama K, Harada H, Tozaki-Saitoh H, Tsuda M, Ushijima K, Inoue K (2011) Astrocytic P2Y(1) receptor is involved in the regulation of cytokine/chemokine transcription and cerebral damage in a rat model of cerebral ischemia. J Cereb Blood Flow Metab 31:1930–1941. CrossRef Medline

Kurth-Nelson ZL, Mishra A, Newman EA (2009) Spontaneous glial calcium waves in the retina develop over early adulthood. J Neurosci 29:11339–11346. CrossRef Medline

Mathiesen C, Brazhe A, Thomsen K, Lauritzen M (2013) Spontaneous calcium waves in Bergman glia increase with age and hypoxia and may reduce tissue oxygen. J Cereb Blood Flow Metab 33:161–169. CrossRef Medline

Monai H, Ohkura M, Tanaka M, Oe Y, Konno A, Hirai H, Mikoshiba K, Itohara S, Nakai J, Iwai Y, Hirase H (2016) Calcium imaging reveals glial involvement in transcranial direct current stimulation-induced plasticity in mouse brain. Nat Commun 7:11100. CrossRef Medline

Navarrete M, Perea G, Fernandez de Sevilla D, Gómez-Gonzalo M, Núñez A, Martin ED, Araque A (2012) Astrocytes mediate in vivo cholinergic-induced synaptic plasticity. PLoS Biol 10:e1001259. CrossRef Medline

Nett WJ, Oloff SH, McCarthy KD (2002) Hippocampal astrocytes in situ exhibit calcium oscillations that occur independent of neuronal activity. J Neurophysiol 87:528–537. CrossRef Medline

Nimmerjahn A, Mukamel EA, Schnitzer MJ (2009) Motor behavior activates Bergmann glial networks. Neuron 62:400–412. CrossRef Medline

Ortinski PI, Dong J, Mungenast A, Yue C, Takano H, Watson DJ, Haydon PG, Coulter DA (2010) Selective induction of astrocytic gliosis generates deficits in neuronal inhibition. Nat Neurosci 13:584–591. CrossRef Medline

Panatier A, Vallée J, Haber M, Murai KK, Lacaille JC, Robitaille R (2011) Astrocytes are endogenous regulators of basal transmission at central synapses. Cell 146:785–798. CrossRef Medline

Pascual O, Ben Achour S, Rostaing P, Triller A, Bessis A (2012) Microglia activation triggers astrocyte-mediated modulation of excitatory neurotransmission. Proc Natl Acad Sci U S A 109:E197–E205. CrossRef Medline

Paukert M, Agarwal A, Cha J, Doze VA, Kang JU, Bergles DE (2014) Norepinephrine controls astroglial responsiveness to local circuit activity. Neuron 82:1263–1270. CrossRef Medline

Rassendren F, Audinat E (2016) Purinergic signaling in epilepsy. J Neurosci Res 94:781–793. CrossRef Medline

Reeves AM, Shigetomi E, Khakh BS (2011) Bulk loading of calcium indicator dyes to study astrocyte physiology: key limitations and improvements using morphological maps. J Neurosci 31:9353–9358. CrossRef Medline

Rungta RL, Bernier LP, Dissing-Olesen L, Groten CJ, LeDue JM, Ko R, Drissler S, MacVicar BA (2016) $Ca^{2+}$ transients in astrocyte fine processes occur via $Ca^{2+}$ influx in the adult mouse hippocampus. Glia 64: 2093–2103. CrossRef Medline

Santello M, Bezzi P, Volterra A (2011) TNFalpha controls glutamatergic gliotransmission in the hippocampal dentate gyrus. Neuron 69:988–1001. CrossRef Medline

Shigetomi E, Bushong EA, Haustein MD, Tong X, Jackson-Weaver O, Kracun S, Xu J, Sofroniew MV, Ellisman MH, Khakh BS (2013) Imaging calcium microdomains within entire astrocyte territories and endfeet with GCaMPs expressed using adeno-associated viruses. J Gen Physiol 141: 633–647. CrossRef Medline

Shigetomi E, Patel S, Khakh BS (2016) Probing the complexities of astrocyte calcium signaling. Trends Cell Biol 26:300–312. CrossRef Medline

Shinozaki Y, Shibata K, Yoshida K, Shigetomi E, Gachet C, Ikenaka K, Tanaka KF, Koizumi S (2017) Transformation of astrocytes to a neuroprotective phenotype by microglia via P2Y1 receptor downregulation. Cell Rep 19:1151–1164. CrossRef Medline

Silverman WR, de Rivero Vaccari JP, Locovei S, Qiu F, Carlsson SK, Scemes E, Keane RW, Dahl G (2009) The pannexin 1 channel activates the inflammasome in neurons and astrocytes. J Biol Chem 284:18143–18151. CrossRef Medline

Sofroniew MV, Vinters HV (2010) Astrocytes: biology and pathology. Acta Neuropathol 119:7–35. CrossRef Medline

Srinivasan R, Huang BS, Venugopal S, Johnston AD, Chai H, Zeng H, Golshani P, Khakh BS (2015) Ca(2+) signaling in astrocytes from Ip3r2(−/−) mice in brain slices and during startle responses in vivo. Nat Neurosci 18: 708–717. CrossRef Medline

Stobart JL, Ferrari KD, Barrett MJ, Stobart MJ, Looser ZJ, Saab AS, Weber B (2018) Long-term in vivo calcium imaging of astrocytes reveals distinct cellular compartment responses to sensory stimulation. Cereb Cortex 28:184–198. CrossRef Medline

Takata N, Mishima T, Hisatsune C, Nagai T, Ebisui E, Mikoshiba K, Hirase H (2011) Astrocyte calcium signaling transforms cholinergic modulation to cortical plasticity in vivo. J Neurosci 31:18155–18165. CrossRef Medline

Tanaka KF, Ahmari SE, Leonardo ED, Richardson-Jones JW, Budreck EC, Scheiffele P, Sugio S, Inamura N, Ikenaka K, Hen R (2010) Flexible Accelerated STOP Tetracycline Operator-knockin (FAST): a versatile and efficient new gene modulating system. Biol Psychiatry 67:770–773. CrossRef Medline

Tan Z, Liu Y, Xi W, Lou HF, Zhu L, Guo Z, Mei L, Duan S (2017) Glia-derived ATP inversely regulates excitability of pyramidal and CCK-positive neurons. Nat Commun 8:13772. CrossRef Medline

Tang W, Szokol K, Jensen V, Enger R, Trivedi CA, Hvalby Ø, Helm PJ, Looger LL, Sprengel R, Nagelhus EA (2015) Stimulation-evoked $Ca^{2+}$ signals in astrocytic processes at hippocampal CA3-CA1 synapses of adult mice are modulated by glutamate and ATP. J Neurosci 35:3016–3021. CrossRef Medline

Thévenaz P, Ruttimann UE, Unser M (1998) A pyramid approach to subpixel registration based on intensity. IEEE Trans Image Process 7:27–41. CrossRef Medline

Ting JT, Daigle TL, Chen Q, Feng G (2014) Acute brain slice methods for adult and aging animals: application of targeted patch clamp analysis and optogenetics. Methods Mol Biol 1183:221–242. CrossRef Medline

Volterra A, Liaudet N, Savtchouk I (2014) Astrocyte Ca(2)(+) signalling: an unexpected complexity. Nat Rev Neurosci 15:327–335. CrossRef Medline

Wu YW, Tang X, Arizono M, Bannai H, Shih PY, Dembitskaya Y, Kazantsev V, Tanaka M, Itohara S, Mikoshiba K, Semyanov A (2014) Spatiotemporal calcium dynamics in single astrocytes and its modulation by neuronal activity. Cell Calcium 55:119–129. CrossRef Medline